We are IntechOpen, the world's leading publisher of Open Access books Built by scientists, for scientists

4,800
Open access books available

122,000
International authors and editors

135M
Downloads

Our authors are among the

154
Countries delivered to

TOP 1%
most cited scientists

12.2%
Contributors from top 500 universities

CLARIVATE ANALYTICS BOOK CITATION INDEX INDEXED

WEB OF SCIENCE™

Selection of our books indexed in the Book Citation Index in Web of Science™ Core Collection (BKCI)

Interested in publishing with us?
Contact book.department@intechopen.com

Numbers displayed above are based on latest data collected.
For more information visit www.intechopen.com

3

Wireless Communication in Tunnels

Jose-Maria Molina-Garcia-Pardo[1], Martine Lienard[2] and Pierre Degauque[2]
[1]*Universidad Politécnica de Cartagena*
[2]*University of Lille, IEMN*
[1]*Spain*
[2]*France*

1. Introduction

A great deal of work is being done to optimize the performances of digital wireless communication systems, and most of the effort is focused on the urban environment where technologies evolve surprisingly fast. Deployment of new emerging technologies, all based on digital communications, first requires the knowledge of the physical layer in order to develop efficient antenna design and communication algorithms. Tunnels, including rail, road and pedestrian tunnels, even if they do not represent a wide coverage zone, must be taken into account in the network architecture, the tunnel either being considered part of a neighboring cell or as a cell itself. In order to cover the tunnel, two solutions have traditionally been proposed: the so-called "natural propagation" using antennas of small size, and leaky coaxial cables. However, the implementation of radiating cables is expensive, at least in long tunnels, because the diameter of the cable must be large enough to avoid a prohibitive attenuation in the 1-5 GHz band, which will be considered in this chapter. We will thus focus our attention on a link based on natural propagation.

Whatever the application, preliminary knowledge of the propagation phenomena is required. The first section of this chapter is thus devoted to a presentation of theoretical models, while in the second section the main narrow band and wideband double-directional channel characteristics, determined from numerous measurement campaigns, will be presented and interpreted. Since Multiple-Input Multiple-Output (MIMO) techniques may strongly improve the spectral efficiency and/or decrease the error rate, keeping the transmitting power and the bandwidth constant; the last two sections will describe their performances in tunnels. Indeed, one can expect the degree of diversity of the channel to be, by far, quite different from its average value in an indoor environment due to the guiding structure of the tunnel. Applying the propagation model to MIMO allows the outlining of the main parameters playing an important role on the ergodic channel capacity, and introducing the so-called modal diversity. From measured channel matrices, predicted capacity is given for various tunnel and array configurations. The last paragraph of this chapter treats the robustness, in terms of error rate, of different MIMO schemes.

2. Modeling the propagation channel

Many approaches have been developed to theoretically study electromagnetic wave propagation inside a tunnel, the most well known being those based either on the ray theory

or on the modal theory (Mahmoud, 1988; Dudley et al., 2007). The transmitting frequency range must be chosen such that the attenuation per unit length is not prohibitive. To fulfill this requirement, the tunnel must behave as an oversized waveguide. Consequently, the wavelength must be much smaller than the transverse dimensions of the tunnel, which leads to transmitting frequencies greater than few hundred MHz in usual road or train tunnels. The objective of this section is to conduct an overview of the techniques to treat tunnels of simple geometry, such as rectangular or circular straight tunnels, by using either the ray theory or the modal theory. Studying wave propagation along such structures will allow simple explanation and interpretation of the experimental results obtained in real tunnels, even of more complicated shapes. Theoretical approaches to treat tunnels of an arbitrary cross-section and/or presenting a series of curves will also be briefly presented.

2.1 Propagation in a straight rectangular tunnel

Let us consider a rectangular tunnel along the z-axis, as shown in Fig. 1, the width and the height of the tunnel being equal to a and b, respectively. The coordinate origin is in the centre of the cross-section, at $z = 0$, which defines the excitation plane. The walls are either characterized by their complex permittivity ε_r^* or by an equivalent conductivity σ and real permittivity ε_r.

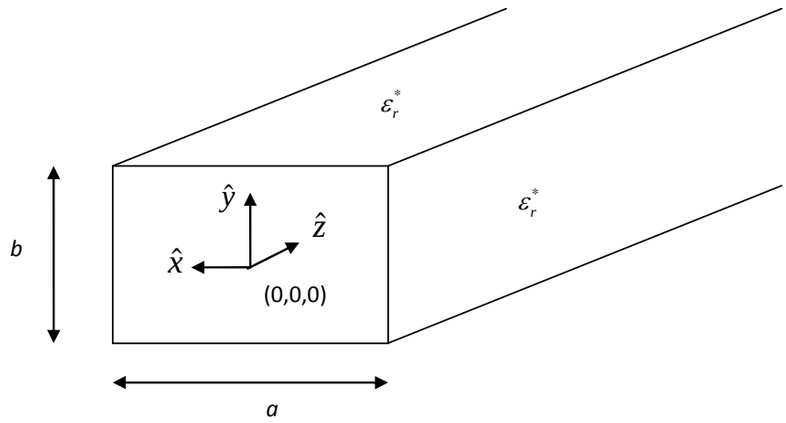

Fig. 1. Geometry of the rectangular tunnel.

2.1.1 Ray theory

Ray theory combined with image theory leads to a set of virtual transmitting (Tx) antennas. If the tunnel is of rectangular cross-section, the determination of the location of these virtual antennas is straightforward, and it is independent of the location of the receiving point. The total field is obtained by summing the contribution of all rays connecting the Tx images and the receiving point (Rx), whilst considering the reflection coefficients on the tunnel walls. However, even by assuming ray propagation, the summation of the contribution of the rays at the Rx point must take into account the vector nature of the electric field. Before each reflection on a wall, the electric field vector must be expressed as the sum of two components: one perpendicular to the incidence plane E_{perp} and one parallel to this plane E_{para}. To each of these components, reflection coefficients R_{TM} and R_{TE} are respectively applied, mathematical expressions for which can be found in any book treating

electromagnetic wave propagation (Wait, 1962; Dudley, 1994). After each reflection, one can thus obtain the new orientation of the electric field vector. The same approach is successively applied by following the rays and by finding the successive incidence planes. Nevertheless, it has been shown (Lienard et al., 1997) that if the distance between Tx and Rx becomes greater than three times the largest dimension of the tunnel cross-section, the waves remain nearly linearly polarized. In this case, the vector summation of the electric field radiated by an antenna and its images becomes a simple scalar summation as in:

$$E(x,y,z) = \sum_m \sum_n \left(R_{TM}\right)^m \left(R_{TE}\right)^n E_d\left(S_{mn}\right) \tag{1}$$

where $E_d\left(S_{mn}\right)$ is the electric field radiated in free space by the image source S_{mn} and corresponding to rays having m reflections on the walls perpendicular to the Tx dipole axis and n reflections on the walls parallel to the dipole axis (Mahmoud & Wait, 1974). In the following examples the excitation by an electric dipole will be considered, but this is not a strong restriction in the ray approach since other kinds of antennas can be treated by introducing their free space radiation pattern into the model, i.e. by weighting the rays in a given direction by a factor proportional to the antenna gain in this direction.

Lastly, it must also be emphasized that the reflection coefficients on the walls tend to 1 if the angle of incidence on the reflecting plane tends to 90°. This means that, at large distances, only rays impinging the tunnel walls with a grazing angle of incidence play a leading part in the received power, thus the number of rays that fulfill this condition is important. Typically, to predict the total electric field in standard tunnels and at distances of a few hundred meters, 20 to 30 rays are needed. One should note that if a base station is located outside the tunnel, and if a mobile moves inside the tunnel, the ray theory can still be applied by taking the diffraction in the aperture plane of the tunnel into account (Mariage et al., 1994).

2.1.2 Modal theory

The natural modes propagating inside the tunnel are hybrid modes EH_{mn}, the three components of the electric and magnetic fields that are present (Mahmoud, 2010; Dudley et al., 2007). Any electric field component $E(x, y, z)$ can be expressed as a sum of the modal components:

$$E(x,y,z) = \sum_m \sum_n A_{mn}\left(0\right) e_{mn}(x,y)\, e^{-\gamma_{mn} z} \tag{2}$$

In this expression, $A_{mn}\left(0\right)$ is the complex amplitude of the mode in the excitation plane, e_{mn} is the normalized modal eigenfunction, and γ_{mn} is the complex propagation constant, often written as $\gamma_{mn} = \alpha_{mn} + j\beta_{mn}$.

It is interesting to introduce the weight of the modes $A_{mn}\left(z\right)$ at any abscissa z by stating:

$$E(x,y,z) = \sum_m \sum_n A_{mn}\left(z\right) e_{mn}(x,y) \quad \text{where} \quad A_{mn}\left(z\right) = A_{mn}\left(0\right)\ e^{-\gamma_{mn} z} \tag{3}$$

The analytical expressions of the modal eigenfunctions are usually obtained by writing the boundary conditions on the internal surface of the guiding structure. However, in the case

of lossy dielectric walls, as in the case of a tunnel, approximations are needed and they are detailed in (Emslie et al., 1975; Laakman & Steier, 1976). We have previously outlined that rays remain polarized if the distance between Tx and Rx is larger than a few times the transverse dimensions of the tunnel. In the modal theory, we have the same kind of approximation. If the tunnel is excited by a vertical (y-directed) dipole, the hybrid modes EH^{y}_{mn} are such that the vertical electric field is dominant. For an x-directed dipole, the modes are denoted EH^{x}_{mn}. The expressions of the modal functions $e^{V}_{mn}(x,y)$ for the y-polarized modes, and $e^{H}_{mn}(x,y)$ for the x-polarized modes can be found in (Mahmoud, 2010; Dudley et al., 2007). The solution of the modal equation leads to expressions for the phase and attenuation constants for the y-polarized modes:

$$\alpha_{mn} = \frac{2}{a}\left(\frac{m\lambda}{2a}\right)^2 \mathrm{Re}\left[\frac{1}{\sqrt{\varepsilon_r^* - 1}}\right] + \frac{2}{b}\left(\frac{n\lambda}{2b}\right)^2 \mathrm{Re}\left[\frac{\varepsilon_r^*}{\sqrt{\varepsilon_r^* - 1}}\right] \text{ and } \beta_{mn} = \frac{2\pi}{\lambda}\left[1 - \frac{1}{2}\left(\frac{m\lambda}{2a}\right)^2 - \frac{1}{2}\left(\frac{n\lambda}{2b}\right)^2\right] \quad (4)$$

From (4), we see that the attenuation is inversely proportional to the waveguide dimension cubed and the frequency squared. It must be stressed that, given the finite conductivity of the tunnel walls, the modes are not precisely orthogonal. Nevertheless, numerical applications indicate that, when considering the first 60 modes with orders m≤ 11 and n≤ 7, the modes can be considered as practically orthogonal (Lienard et al., 2006; Molina-Garcia-Pardo et al., 2008a). As an example, let us consider a tunnel whose width and height are equal to 4.5 m and 4 m, respectively, and whose walls are characterized by an equivalent conductivity σ = 10^{-2} S/m and a relative real permittivity ε_r = 10. Table 1 gives the attenuation, expressed in dB/km, of the first $EH_{m,n}$ hybrid modes and for two frequencies 2.4 GHz and 10 GHz.

	n=1	n=2	n=3		n=1	n=2	n=3
m=1	4.6 dB	17 dB	38 dB	m=1	0.2 dB	0.8 dB	1.8 dB
m=2	6 dB	18 dB	40 dB	m=2	0.3 dB	0.9 dB	1.9 dB
m=3	8 dB	21 dB	42 dB	m=3	0.4 dB	1 dB	2 dB
f = 2.4 GHz.				f = 10 GHz			

Table 1. Attenuation along 1 km of the various $EH_{m,n}$ hybrid modes

At 10 GHz, the fundamental mode exhibits a negligible attenuation, less than 0.2 dB/km, while at 2.4 GHz it is in the order of 5 dB/km. Two other points must be outlined. First, if we consider, for example, a frequency of 2.4 GHz, and a distance of 1 km, one can expect that only 2 or 3 modes will play a leading part in the total received signal, while at 10 GHz, a large number of modes will still be present, the attenuation constant being rather low. This leads to the concept of the number N_a of "active modes" significantly contributing to the total power at the receiver, and which will be extensively used in 4.1 to predict the capacity of multiantenna systems such as MIMO. To simply show the importance of introducing these active modes, let us recall that the phase velocity of the waves differs from one mode to another. Interference between modes occurs, giving rise to fluctuations in the signal both along the z-axis and in the transverse plane of the tunnel. One can expect that at 1 km, the fluctuations at 10 GHz will be more significant and rapid than at 2.4 GHz, taking the large number of "active modes" into account. Similarly, for a given frequency N_a continuously decreases with the distance between Tx and Rx. Variations in the field components will thus

be more pronounced in the vicinity of Tx. This phenomenon will have a strong impact on the correlation between array elements used in MIMO systems.

For a vertical transmitting elementary dipole situated at (x_{tx}, y_{tx}), the total electric field at the receiving point (x, y, z) can be determined from (Molina-Garcia-Pardo et al., 2008c):

$$E(x,y,z) = \sum_m \sum_n e^V_{m,n}(x_{tx}, y_{tx})\, e^V_{m,n}(x,y)\, e^{-\gamma_{m,n} z} \tag{5}$$

To treat the more general case of a radiating structure presenting a radiation pattern which is assumed to be known in free space, the easiest solution to determine the weight of the modes in the Rx plane is to proceed in two steps. First, the E field in the tunnel is calculated numerically using, for example, the ray theory, and then the weight $A_{m,n}(z)$ of any mode m,n for this abscissa can be obtained by projecting the electric field on the basis of $e^V_{mn}(x,y)$ (Molina-Garcia-Pardo et al., 2008a). This leads to:

$$A_{mn}(z) = \int_{-a/2}^{a/2} \int_{-b/2}^{b/2} E(x,y,z) \cdot e^V_{mn}(x,y)\, dx dy \tag{6}$$

In the following numerical application a 8 m-wide, 4.5 m-high tunnel is considered, the electrical parameters of the walls being $\sigma = 10^{-2}$ S/m and $\varepsilon_r = 5$. The radiating element is a vertical elementary dipole situated 50 cm from the ceiling, at 1/4 of the tunnel width, and the transmission frequency is 900 MHz. This configuration could correspond to a practical location of a base station antenna in a real tunnel. The six modes with the highest energies at a distance of 300 m and 600 m are provided in Table 2.

Modes	2,1	1,1	3,1	5,1	6,1	2,2
300 m	0 dB	-2 dB	-3 dB	-4 dB	-4 dB	-5 dB
600 m	0 dB	-2 dB	-4 dB	- 9 dB	-9 dB	-15 dB

Table 2. Relative weights of the modes at 300 m and 600 m.

Due the non-centered position of the Tx dipole, the most energetic mode is mode 2,1, although mode 1,1 is the lowest attenuated. The other columns in Table 2 show the relative weight of the other modes, normalized for each distance in terms of the highest mode weight, i.e. mode 2,1. At 300 m, numerous other modes are still significantly contributing to the total field, since the 6th mode only presents a relative attenuation of 5 dB in relation to the strongest mode. On the other hand, at 600 m only a few higher-order modes remain. The application of such an approach for predicting the performance of MIMO systems will be used in 4.1 and 4.2.

2.2 Propagation in a straight circular tunnel

Even if a perfectly circular tunnel is less usual, it is interesting to outline some specific features related to the modes and polarization of the waves propagating in such a guiding structure. A detailed analysis (Dudley et al., 2007) shows that an elementary electric dipole produces a large set of modes, the possible modes being TE_{0m}, TM_{0m} and the hybrid modes EH_{nm} and HE_{nm}.

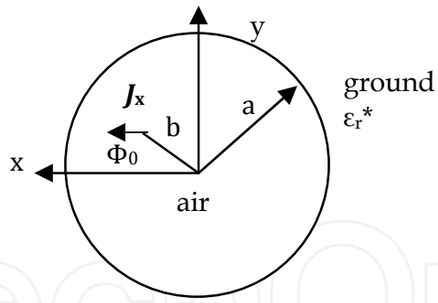

Fig. 2. Configuration of a cylindrical tunnel and location of a transmitting antenna.

An important feature of the propagation phenomena for MIMO communication systems based on polarization diversity is the cross polarization discrimination factor, XPD, defined as the ratio of the co-polarized to the cross-polarized average received power. Indeed, as will be outlined in 3.1.2, XPD quantifies the separation between two transmission channels that use different polarization orientations. In a circular tunnel and assuming a x-oriented dipole *Jx* at $(b,\phi_0,0)$, it can be shown (Dudley et al., 2007) that the cross-polar fields at an observation point (ρ,ϕ,z) vanish at $\phi_0 = 0,\pi/2$ but are maximum at $\phi_0 = \pi/4$. In this last case, if the observation point is at the same circumferential location as the source point, XPD becomes equal to 1. The polarization of the waves in a circular tunnel is thus quite different than in a rectangular tunnel, where, at large distances, the co-polarized field component is always dominant.

In practice, the shape of a tunnel is often neither perfectly circular nor rectangular. Consequently, numerous measurement campaigns have been carried out in different tunnel configurations and the results, compared to the theoretical approach based on simplified shapes of tunnel cross-sections, are presented in 3.2. However, before presenting narrow band and wideband channel characteristics in a real tunnel, the various methods for numerically treating propagation in tunnels of arbitrary shape will be briefly described.

2.3 Propagation in a tunnel of arbitrary shape

If we first consider a bent tunnel of rectangular cross-section whose radius of curvature is much larger than the transverse dimensions of its cross-section, approximate solutions of the modal propagation constants based on Airy function representation of the fields have been obtained (Mahmoud, 2010). For an arc-shaped tunnel, the deviation of the attenuation and the phase velocity of the dominant modes from those in a perfectly rectangular tunnel are treated in (Mahmoud, 2008) by applying a perturbation theory. Lastly, let us mention that for treating the propagation in tunnels of arbitrary shapes, various approaches have recently been proposed, despite the fact that they are more complicated to implement and that the computation time may become prohibitive for long-range communication. Ray launching techniques and ray-tube tracing methods are described in (Didascalou et al., 2001) and in (Wang & Yang, 2006), the masking effect of vehicles or trains being treated by introducing additional reflection/diffraction on the obstacle. A resolution of the full wave Maxwell equations in the time domain through a high order vector finite element discretization is proposed in (Arshad et al., 2008), while solutions based on the parabolic equation and spectral modeling are detailed in (Popov & Zhu, 2000). We will not describe in detail all these methods, since the objective of this chapter is to present the general behavior of the propagation in tunnels, rather than to emphasize solutions to specific problems.

3. Narrow band and wideband channel characterization

As previously outlined, a number of propagation measurements in tunnels have been taken over the last 20 years, and it is not within the scope of this chapter to make an extensive overview of what has been done and published. Let us simply mention that the results cover a wide area of environment and applications, starting from mine galleries (Lienard & Degauque, 2000a; Zhang et al., 2001; Boutin et al. 2008), road and railway tunnels (Lienard et al., 2003; Lienard et al., 2004), pedestrian tunnels (Molina-Garcia-Pardo et al., 2004), etc. We have thus preferred to select one or two scenarios throughout this chapter in order to clearly identify the main features of the propagation phenomena and their impact on the optimization of the transmission scheme.

3.1 Narrow band channel characteristics

We first consider the case of a rectangular tunnel for applying the simple approach described in the previous sections and for giving an example of path loss versus the distance between Tx and Rx. Then, results of the experiments carried out in an arched tunnel will be presented and we will study the possibility of interpreting the measurements from a simple propagation model, i.e. by means of an equivalent rectangular tunnel.

3.1.1 Path loss determined from a propagation model in a rectangular tunnel

Let us consider a wide rectangular, 13 m wide and 8 m high, corresponding to the transverse dimensions of a high-speed train tunnel. Curve (a) in Fig. 3 represents the variation of the field amplitude, expressed in dB and referred to an arbitrary value, versus the distance *d*, which is determined from the theoretical approach based on the ray theory. The transmitting frequency is 2.1 GHz and the Tx antenna is supposed to be a half-wave dipole situated at a height of 2 m and at a distance of 2 m along a vertical wall.

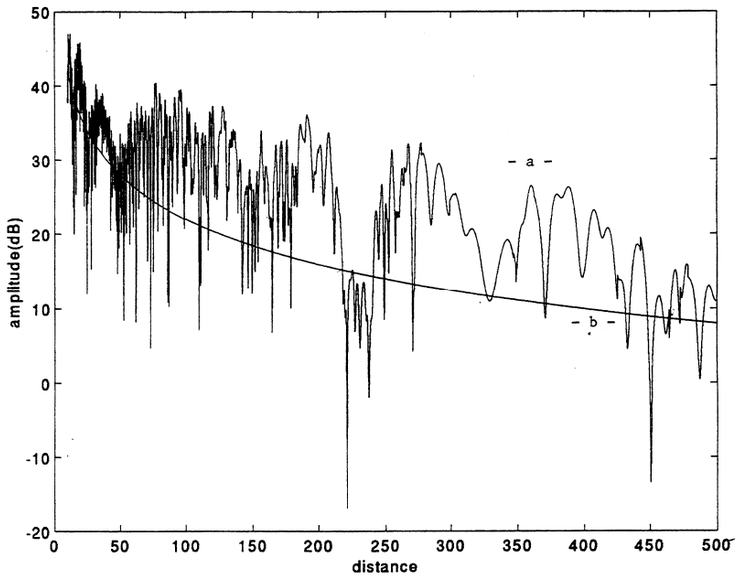

Fig. 3. a) Amplitude of the received signal, referred to an arbitrary value, determined from the ray theory in a rectangular tunnel. b) Amplitude of the signal for a free space condition (Lienard & Degauque, 1998).

The walls have a conductivity of 10^{-2} S/m and a relative permittivity of 10. As a comparison, curve (b) corresponds to the case of free space propagation. Along the first 50 m the field amplitude decreases rapidly, in the order of 5 dB/100 m, and fast fluctuations can be observed. They are due to the interference between the numerous paths relating Tx and Rx or, from the modal theory point of view, to interference between modes. Beyond this distance d_1 of 50 m, we note a change in the slope of the path loss which becomes equal to 1 dB/100 m. A two-slope model is thus well suited for such a tunnel and is also detailed in (Marti Pallares et al., 2001; Molina-Garcia-Pardo et al., 2003). In general, the abscissa of the break point d_1 depends on the tunnel excitation conditions and hence, on the position of the Tx antenna in the transverse plane, and on its radiation pattern. For a longer transmission range, a three/four-slope model has also been proposed (Hrovat et al., 2010).

After having determined the regression line in each of the two intervals and subtracted the effect of the average attenuation, one can study the fading statistics. Usually, as in an urban environment, the fading is divided into large scale and small scale fading, by considering a running mean on a few tens of wavelengths (Rappaport, 1996). However, in a straight tunnel, making this distinction between fading cannot be related to any physical phenomena. Furthermore, as it appears from curve 3a, the fading width and occurrence depend on the distance. An analysis of the fading characteristics is given in (Lienard and Degauque, 1998). Let us mention that the masking effect due to traffic in road tunnels or to trains in railway tunnels are detailed in (Yamaguchi et al., 1989; Lienard et al., 2000b; Chen et al., 1996, 2004).

3.1.2 Experimental approach to propagation in an arched tunnel and the concept of an equivalent rectangular tunnel

Numerous measurements have been carried out in the tunnel shown in Fig. 4a and 4b. The straight tunnel, 3 km-long, was closed to traffic during the experiments. The walls are made of large blocks of smooth stones. It is difficult to estimate the roughness accurately, but it is in the order of a few millimeters. In a first series of experiments, the transmitting power was 34 dBm

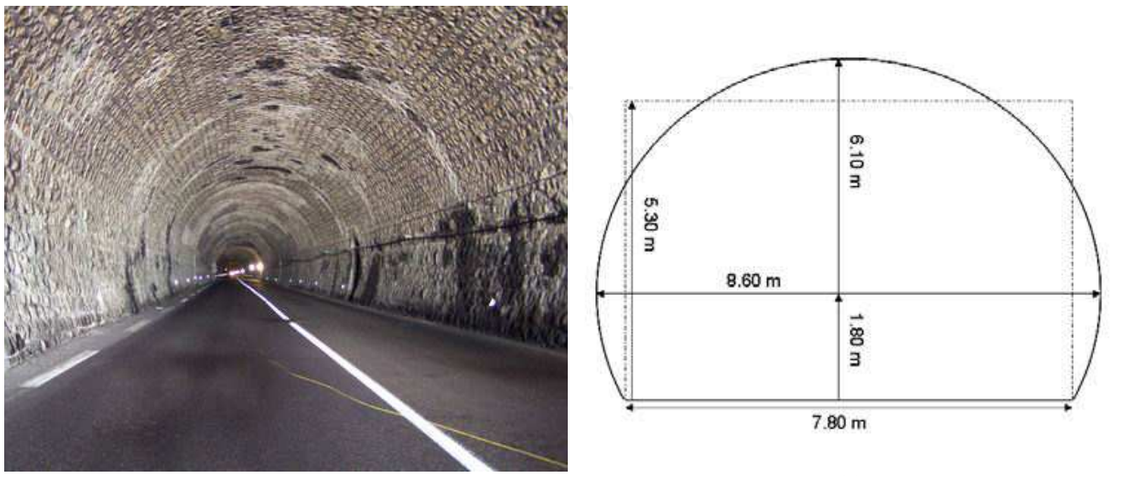

a) b)

Fig. 4. a) Photo of the tunnel where measurements took place; b) Cross-section of the tunnel.

and the Tx and Rx half-wave dipole antennas were at the same height (2 m) and centered in the tunnel. Curves in Fig. 5 show the variation in the received power at 510 MHz, versus the axial distance *d* between Tx and Rx, the Tx and Rx antennas being both horizontally (HH) or vertically (VV) polarized (Molina-Garcia-Pardo et al., 2008b).

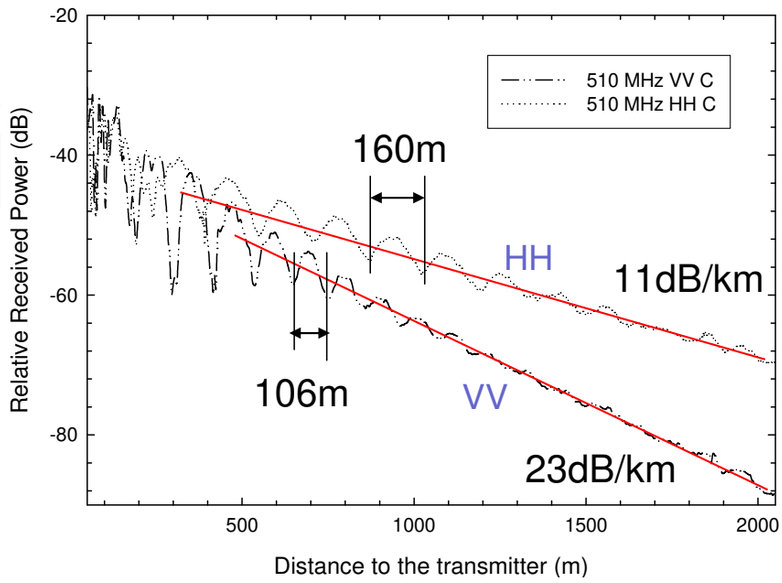

Fig. 5. Received power (dBm) in the arched tunnel for two polarizations at 510 MHz (Molina-Garcia-Pardo et al., 2008b).

We first note that the slope of the path loss is much higher for the VV polarization than for HH. Furthermore, if *d* becomes greater than 500 m, the spatial fading becomes periodic, but the periodicity is not the same for HH (160 m) and for VV (106 m). Since such results, showing a lack of cylindrical symmetry, cannot be interpreted with a simple model based on a cylindrical structure, we have tried to find the transverse dimensions of a rectangular tunnel, equivalent to the actual arched tunnel, which minimize the difference between the theoretical and experimental values. The choice of a rectangular cross-section whose surface is nearly equal to the surface of the actual tunnel seemed to be relevant. It appears that the best results were obtained for a rectangle 7.8 m wide and 5.3 m high, as shown in Fig. 4 b, the electrical characteristics of the walls being $\sigma = 10^{-2}$ S/m and $\varepsilon_r = 5$. To be useful, this equivalent rectangle must still be valid for other frequencies or configurations. As an example, let us now consider a frequency of 900 MHz, a vertical polarization (VV), both Tx and Rx vertical antennas being either centered in the tunnel (position noted C) or not centered (NC), i.e. situated at ¼ of the tunnel width (Molina-Garcia-Pardo et al., 2008c). Curves in Fig. 6 show the relative received power in dB (normalized to an arbitrary value) at 900 MHz for the two positions of the antennas ("C" and "NC") either measured or determined from the modal theory. In the theoretical modeling, only the first two dominant modes have been taken into account (EH_{11} and EH_{13} for "C", EH_{11} and EH_{12} for "NC").

A rather good agreement is obtained at large distance from Tx, where high order modes are strongly attenuated. The last point which can be checked before using the concept of equivalent rectangular tunnel, deals with the polarization of the waves at a large distance

from Tx, cross-polar components appearing for critical positions of the Tx and Rx antennas in a circular tunnel, while in a rectangular tunnel the waves always remain polarized. Other measurements were made by placing the Tx and Rx antennas in the transverse plane at the critical location where XPD=1 in a circular tunnel ($\phi_0 = \pi / 4$ in Fig. 2). As detailed in Molina-Garcia-Pardo et al. (2008c), the experiments show that the waves remain polarized. The simple model of the propagation in an equivalent rectangular tunnel seems thus quite suitable to predict and/or justify the performances of communication systems using, for example, MIMO techniques, as described in 4.1 and 4.2.

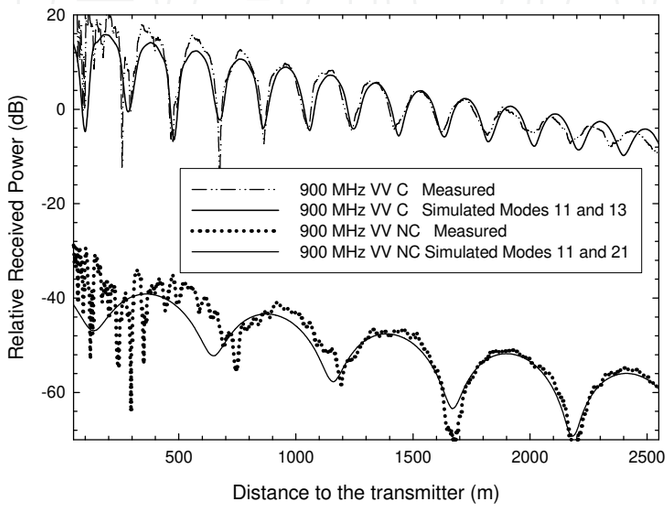

Fig. 6. Relative received power (dB) at 900 MHz for two configurations either measured or determined from the modal theory taking only two modes into account (Molina-Garcia-Pardo et al., 2008c).

3.2 Wideband and double directional channel characteristics

For optimizing the transmission scheme and predicting the performance of the communication link, the channel is characterized in the frequency domain by the coherence bandwidth B_c defined as the bandwidth over which the frequency correlation function is above a given threshold (Rappaport, 1996; Molisch, 2005), and in time domain by the delay spread D_S determined from the power delay profile (PDP). In the new generation of transmission schemes as in MIMO, double directional channel characteristics, such as the direction of arrival (DOA) and the direction of departure (DOD) of the rays are interesting to analyze since they have a strong impact on the optimization of the antenna arrays. We will successively present these characteristics established either from a propagation model or from measurements.

3.2.1 Characteristics determined from a propagation model in a rectangular tunnel

It has been previously outlined that, at a short distance from Tx, numerous modes or a large number of rays contribute to the total field. At a given distance of Tx, the number of active modes increases with the transverse dimensions of the tunnel, the attenuation of the EH_{mn} modes being a decreasing function of the width or of the height as shown in (4). If the tunnel width increases, interference between modes or rays will give a more rapidly fluctuating field with frequency, and thus a decrease in the coherence bandwidth B_c. As an example, for

a frequency of 2.1 GHz in a tunnel 8 m high, B_C decreases from 40 MHz to 15 MHz when the tunnel width increases from 5 m to 20 m. The channel impulse response (CIR) can be established from the channel transfer function calculated in the frequency domain by applying a Hamming window, for example, and an inverse Fourier transform. In Fig. 7, for a tunnel 13 m wide and 8 m high and a bandwidth of 700 MHz, the theoretical amplitude of the received signal in a delay-distance representation has been plotted, in reference to an arbitrary level and using a color scale in dB. At a given distance, the successive packets of pulses, associated with reflections on the walls, clearly appear. We also see that the excess delay is a decreasing function of distance.

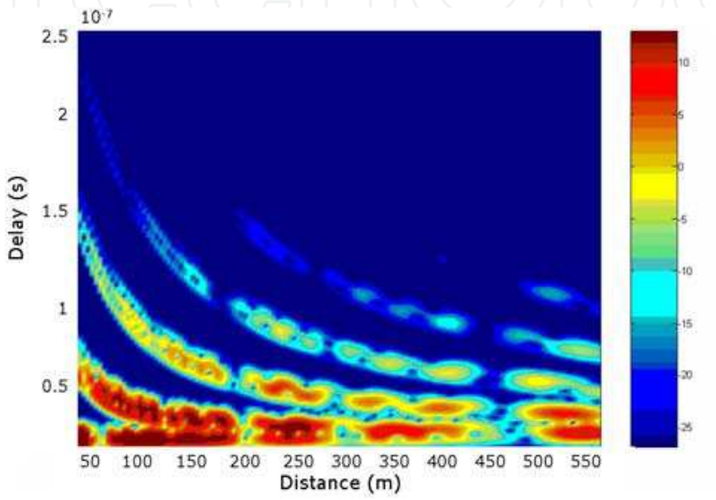

Fig. 7. Theoretical channel impulse response in a wide rectangular tunnel.

At first glance, one could conclude that the excess delay is a decreasing function of distance. However, a more interesting parameter is the delay spread, D_S, defined as the second-order moment of the *CIR* (Molisch, 2005). It is calculated at each distance d by normalizing each CIR to its peak value. For a threshold level of -25 dB, D_S varies in this wide tunnel, between 5 and 28 ns, but the variation is randomly distributed when 50 m < d < 500 m. From the theoretical complex CIRs, the DOA/DOD of the rays can be calculated by using high resolution algorithms such as SAGE or MUSIC (Therrien, 1992). At a distance d of 50 m, the angular spectrum density determined from MUSIC is plotted in Fig. 8. It represents the diagram (delay, DOA), each point being weighted by the relative amplitude of the received signal, expressed in dB above an arbitrary level, and conveyed in a color scale. The DOA is referred to the tunnel axis.

At a distance of 50 m, the rays arriving at an angle greater than 50° are strongly attenuated. A parametric study shows that the angular spread is a rapidly decreasing function of the distance d. This can be easily explained by the fact that rays playing a dominant role at large distances, impinging the tunnel walls with a grazing angle of incidence.

3.2.2 Characteristics determined from measurements in an arched tunnel

Measurement campaigns in the 2.8-5 GHz band have been carried out in the arched tunnel described in 3.1.2. The channel sounder was based on a vector network analyser (VNA) and on two virtual linear arrays. More details on the measurement procedure can be found in

(Molina-Garcia-Pardo et al., 2009c, 2009d). The mean delay spreads are given in Table 3, calculated in 5 successive zones, from 100 m to 500 m from Tx. As shown in Table 3, the delay spread in this range of distance remains nearly constant, in the order of a few ns, whatever the distance d. This result is strongly related to the DOA/DOD of the rays. The variation in their angular spread A_s is plotted in Fig. 9. At 50 m, A_s is equal to about 12° and then decreases with distance (Garcia-Pardo et al., 2011).

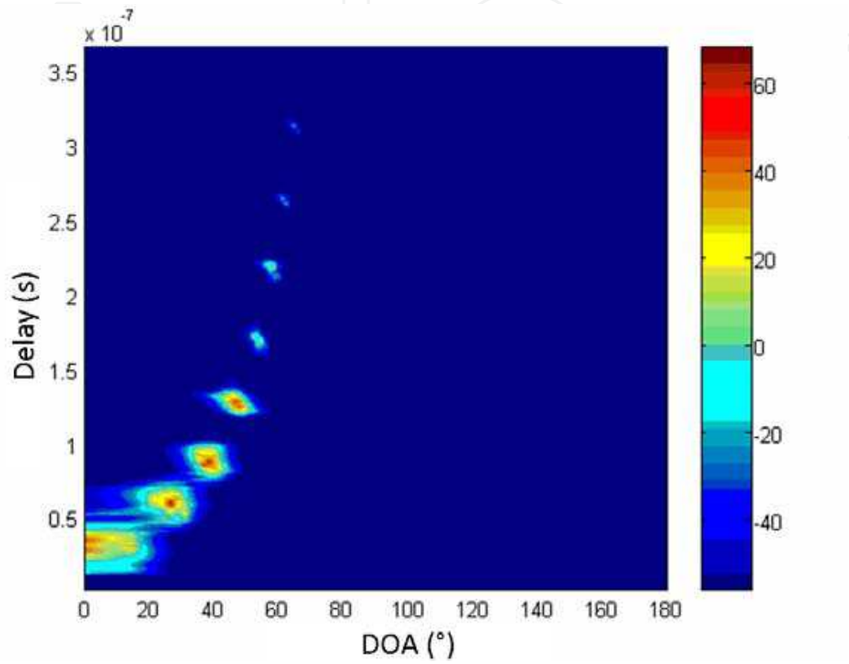

Fig. 8. Theoritical angular power spectrum of the DOA in the plane (delay, direction of arrival), in a wide tunnel and at 50 m from the transmitter.

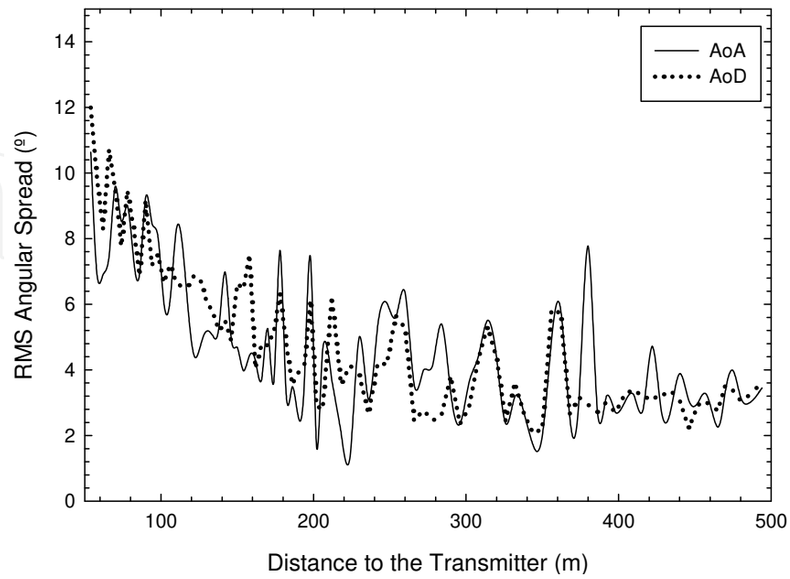

Fig. 9. Angular spread of the DOA/DOD of the rays in a road tunnel (Garcia-Pardo et al., 2011).

Distance (m)	100	200	300	400	500
Mean delay spread (ns)	2.5	1.7	2	1.8	2

Table 3. Mean delay spread in a semi arched road tunnel.

The fact that the delay spread remains constant can thus be explained by this decrease of A_s leading to constant time intervals between successive rays. Other measurements carried out in curved tunnels or tunnels presenting a more complex structure are reported for example in (Wang & Yang, 2006; Siy et al., 2009).

4. MIMO communications in tunnels

To improve the performances of the link, one of the most effective approaches recently developed is based on MIMO techniques (Foschini & Gans, 1998). Enhancement of spectral efficiency and/or decrease of the bit error rate (BER) were clearly emphasized for indoor environments, but in this case the paths between the Tx and Rx array elements are not strongly correlated (Correia, 2006). In a tunnel, however, the DOA/DOD of the rays are not widely spread, and one can wonder whether the number of active modes produce both a sufficient spatial decorrelation and a distribution of the singular values of the $\boldsymbol{H}$ matrix so that space time coding will yield a significant increase in the channel capacity.

4.1 Prediction of capacity from propagation models

To compute the elements of the $\boldsymbol{H}$ matrix, ray theory can be applied by adding all complex amplitudes of the rays received at each Rx antenna, this process being repeated for all Tx antennas. However, the computational cost increases when the receiver is placed far from Tx since the number of reflections needed to reach convergence becomes very large. A more interesting approach is the modal theory (Kyritsi & Cox, 2002; Molina-Garcia-Pardo et al., 2008a). In an *M*×*N* MIMO system (*M* being the number of Tx antennas and *N* the number of Rx antennas), the *Nx1* received signal $\vec{\boldsymbol{y}}$ is equal to:

$$\vec{\boldsymbol{y}} = \boldsymbol{H}\vec{\boldsymbol{x}} + \vec{\boldsymbol{n}} \tag{7}$$

where $\vec{\mathbf{x}}$ is the *Mx1* transmitted vector and $\vec{\mathbf{n}}$ is the *Nx1* additive white Gaussian noise vector. The transfer matrix $\boldsymbol{H}$ is fixed, i.e. deterministic, for any given configuration. The capacity for a given channel realization is given by (Telatar, 1995; Foschini & Gans, 1998):

$$C = \log_2\left(\det\left(\boldsymbol{I}_N + \frac{SNR}{M}\boldsymbol{H}\boldsymbol{H}^{\dagger}\right)\right) = \sum_{i=1}^{\min(N,M)} \log_2\left(1 + SNR\,\lambda_i\right) \tag{8}$$

where $\boldsymbol{I}_N$ is the *N*x*N* identity matrix, † represents the conjugate transpose operation, λ_i are the normalized eigenvalues of $\boldsymbol{H}\boldsymbol{H}^{\dagger}$ and *SNR* is the signal-to-noise ratio at the receiver. Let $A_{mn}^{j}(z)$ be the amplitude of the mode produced by the j^{th} transmitting array element at the receiving axial location *z*. Each term $h_{ij}(z)$ of $\boldsymbol{H}$, is the transfer function between the Tx element *j* and the Rx element *i*. This transfer function can be easily determined from (3):

$$h_{ij}(z) = \sum_{j=1}^{M} \sum_{m} \sum_{n} A_{mn}^{j}(z)\, e_{mn}(x_i, y_i) \;= \sum_{j=1}^{M} \sum_{m} \sum_{n} A_{mn}^{j}(0)\, e_{mn}(x_i, y_i)\; e^{-\gamma_{mn} z} \tag{9}$$

In the above summation, the two terms $A_{mn}^{j}(z)$ and $e_{mn}(x_i, y_i)$ are functions of the position of the Tx element and of the Rx element of coordinates (x_i, y_i), respectively. We note that if the two sets of modes excited by two transmitting elements j_1 and j_2 have the same relative weight, two columns of $\boldsymbol{H}$ become proportional. In this case, $\boldsymbol{H}$ is degenerated and spatial multiplexing using these elements is no longer possible. In (Molina-Garcia-Pardo et al., 2008a), two rectangular tunnels were considered, with transverse dimensions 8 m × 4.5 m (large tunnel) and 4 m × 4.5 m (small tunnel). One conclusion of this work is that the Tx antenna must be off-centered, so that a large number of modes are excited with nearly similar weights, contrary to the case of an excitation by a centered element. Numerical applications show that, at a distance of 600 m and for an excitation by an antenna offset of 1/4 of the tunnel width, there are five modes whose relative amplitudes, when referred to the most energetic mode, are greater than -7 dB, whereas for the centered source, there are only three modes. In the following, we thus consider off-centered source positions, in order to excite a large number of active modes. Another limiting factor in MIMO performance is the correlation between receiving array elements (Almers et al., 2003). As an example, assume that the transmitting array is situated at 1/4 of the tunnel width and at 50 cm from the ceiling. For the two previous tunnels, we calculate the average spacing Δx that produces a correlation coefficient ρ, between vertical electric fields at x and $x+\Delta x$, smaller or equal to 0.7. Results in Fig. 10 show that the correlation distance is an increasing function of the axial distance, due to the decrease in the number of active modes.

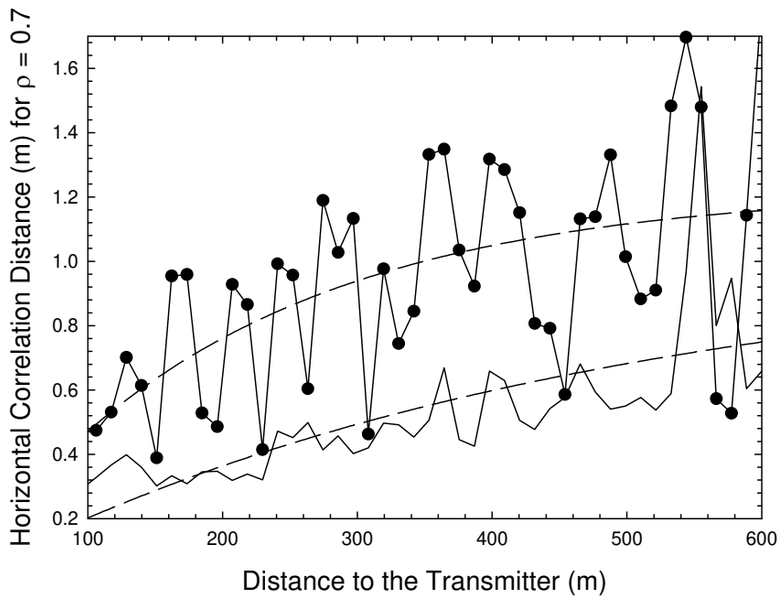

Fig. 10. Horizontal correlation distance (for ρ = 0.7) for two tunnels for a frequency of 900 MHz. Curve with successive points deals with the tunnel 8 m wide, the other curve corresponds to the tunnel 4.5 m wide, the dashed lines give the averaged values (Molina-Garcia-Pardo et al., 2008a).

One can also calculate the correlation $\rho^{E}_{j_1 j_2}(z)$ between the electric fields received in a transverse plane, when the transmitting elements are j_1 and j_2, successively. Mathematical expressions of this correlation function are given in (Molina-Garcia-Pardo et al., 2008a), these authors also introduce a correlation function between modes. An example is given in Fig. 11, where the variation of $\rho^{E}_{j_1 j_2}(z)$ for the large tunnel is plotted. We observe that, as expected, $\rho^{E}_{j_1 j_2}(z)$ increases with distance. It is strongly dependent on the spacing between the Tx elements, and especially when this spacing becomes equal or smaller than 2λ.

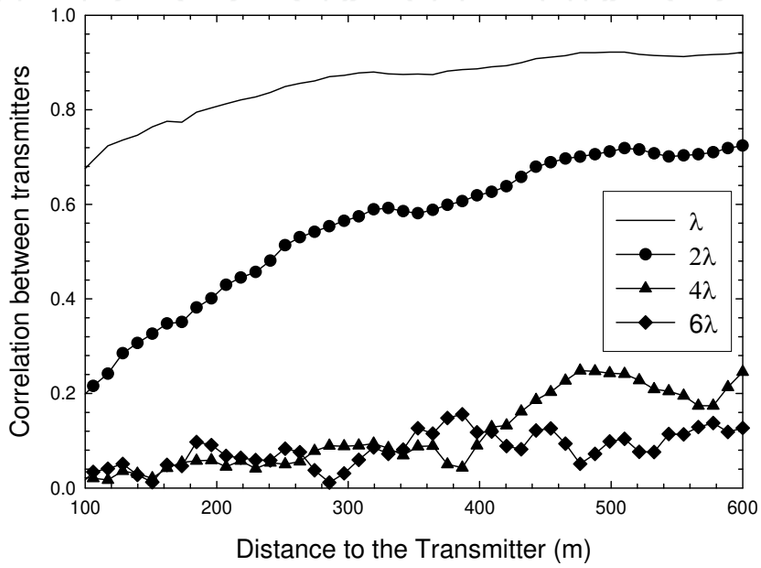

Fig. 11. Average correlation between the electric fields produced by two transmitters in the large tunnel for different array element spacing (6λ, 4λ, 2λ and λ) (Molina-Garcia-Pardo et al., 2008a).

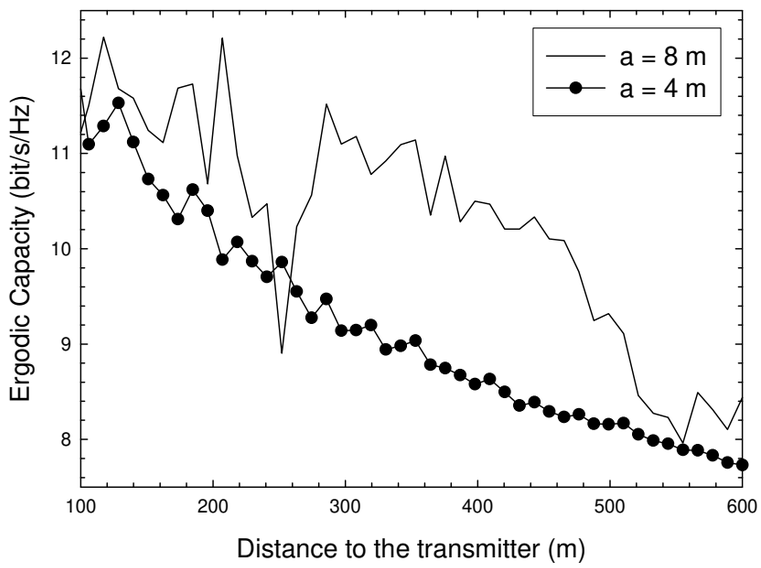

Fig. 12. Capacity of a 4x4 MIMO system for a *SNR* of 10 dB in both tunnels (Molina-Garcia-Pardo et al., 2008a).

Finally, the theoretical ergodic capacity *C*, calculated for an *SNR* of 10 dB versus distance, is presented in Fig. 12 for the two tunnel widths. At short distances, important fluctuations in *C* are found in the large tunnel due to the great number of active modes. In the small tunnel, due to the reduction in the number of modes and of correlation effects, *C* is smaller. For the same reason, we observe that in both tunnels, *C* is a continuously decreasing function of distance. We have thus seen that the concept of spatial diversity usually used in MIMO must be replaced, in tunnels, by the concept of modal diversity, the problem being to optimize the antenna array to excite numerous modes and thus to guarantee a low correlation between the multipath channels.

To conclude this section, it is interesting to have a measure of the multipath richness of the tunnel, and thus of the capacity, independent of the number of array elements. Therefore, we define a reference scenario corresponding to a uniform excitation of the tunnel and to a recovery of all modes in the Rx plane. This can be theoretically achieved by putting, in the whole transverse plane of the tunnel, a two-dimensional (2D) equal-space antenna array with inter-element spacing smaller that $\lambda/2$ (Loyka, 2005). In such a reference scenario, even if unrealistic from a practical point of view, each eigenvalue λ_i corresponds to the power P_{mn} of a mode EH_{mn} in the receiving plane (Molina-Garcia-Pardo et al., 2009a, 2009b). In this case, the capacity $C^{ref\,sce}$ in this scenario is given by:

$$C^{ref\,sce} = \lim_{k\to\infty}\left[\sum_{i=1}^{k}\log_2\left(1+SNR\,\Lambda_i^{ref\,sce}\right)\right] \text{ with } \Lambda_i^{ref\,sce} = \frac{\exp\left(2(\alpha_{11}-\alpha_{mn})z\right)}{\sum_{m,n}\exp\left(2(\alpha_{11}-\alpha_{mn})z\right)} \qquad (10)$$

$C^{ref\,sce}$ only depends on the *SNR* and on the attenuation constants α_{mn} of the modes and thus on the frequency and on the electrical and geometrical characteristics of the tunnel.

Fig. 13 shows the variation in $C_k^{ref\,sce}$ versus the number *k* of eigenvalues of $\boldsymbol{H}$ or of the modes taken into account, the modes being sorted in decreasing power, for different frequencies between 450 and 3600 MHz. The distance between Tx and Rx is 500 m. At 450 MHz, only one mode mainly contributes to the capacity, and at 900 MHz the capacity still rapidly converges to its real value, since high order modes are strongly attenuated. At 1800 MHz, the summation must be made on at least 10 modes, since the attenuation constant in a smooth rectangular tunnel decreases with the square of frequency. At 3600 MHz, the attenuation of the first 30 modes is rather small and it appears that the curve nearly fits the curve "Rayleigh channel" plotted by introducing i.i.d. values as entries for the $\boldsymbol{H}$ matrix.

Finally, for this reference scenario and for a frequency of 900 MHz, Table 4 gives the number of modes needed to reach 90% of the asymptotic value of the capacity at different distances. It clearly shows the decreasing number of modes playing a leading part in the capacity when increasing the distance.

Distance Tx-Rx	d = 125 m	d = 250 m	d = 500 m	d = 1000 m
Number of modes	8	5	3	2

Table 4. Number of modes needed to reach 90% of the asymptotic value of the capacity at 900 MHz and for different distances.

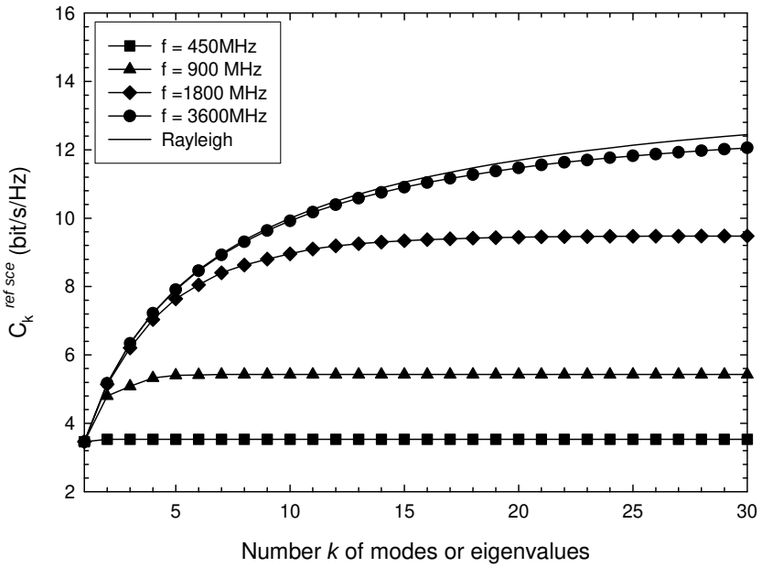

Fig. 13. Capacity $C_k^{ref\ sce}$ for the reference scenario versus the number k of eigenvalues or modes taken into account. The distance between Tx and Rx is 500 m, the tunnel being 5 m wide and 4 m high (Molina-Garcia-Pardo et al., 2009b).

To sum up this section, let us recall that the excitation of the modes plays a leading part in MIMO systems. It is thus interesting to excite the maximum number of modes, with nearly the same amplitude at the receiver plane. Optimum array configurations must thus be designed to obtain the maximum profit from MIMO systems. Furthermore, changes to the tunnel shape, such as narrowing or curves, will modify the weight of the modes and consequently the MIMO performance, as we will see in the next section.

4.2 MIMO channel capacity determined from experimental data

As stated before, many experiments have been conducted in mines and tunnels to extract both narrowband and wideband channel characteristics, but MIMO aspects were only recently considered. To illustrate both the interest of using MIMO in tunnels and the limitation of this technique, two scenarios are successively considered. First, the expected capacity will be determined from measurement campaigns in a subway tunnel whose geometry is rather complicated. Then we will consider the straight road arched tunnel discussed in 3.1.2, and whose photo is given in Fig. 4, to discuss the interest or not of using polarization diversity in conjunction with MIMO systems. Other studies, published in the literature, deal with pedestrian tunnels (Molina-Garcia-Pardo et al., 2003, 2004) where the position of the outside antenna is critical for the performance of the system. More recently, investigations into higher frequency bands have been carried out either for extracting double directional characteristics in road tunnels (Siy Ching et al., 2009), or for analyzing the performance of MIMO in the Barcelona Metro (Valdesuerio et al., 2010).

4.2.1 MIMO capacity in a subway tunnel

Measurements were made along the subway line, shown in Fig. 14, between two stations, Quai Lilas and Quai Haxo, 600 m apart (Lienard et al., 2003). The geometrical configuration

can be divided into two parts: Firstly, there is a two-track tunnel that exhibits a significant curve along 200 m, from Lilas (point A) to point B, and then the tunnel is straight from point B to point D (100 m apart). Beyond this point and up to Haxo, the tunnel is narrow, becoming a one-track tunnel for the last 300 m (from D to C). The width of the one-track and of the two-track tunnel is 4 m and 8 m, respectively. The height of the tunnel is 4.5 m. Its cross-section is arched, but numerous cables and equipment are supported on the walls.

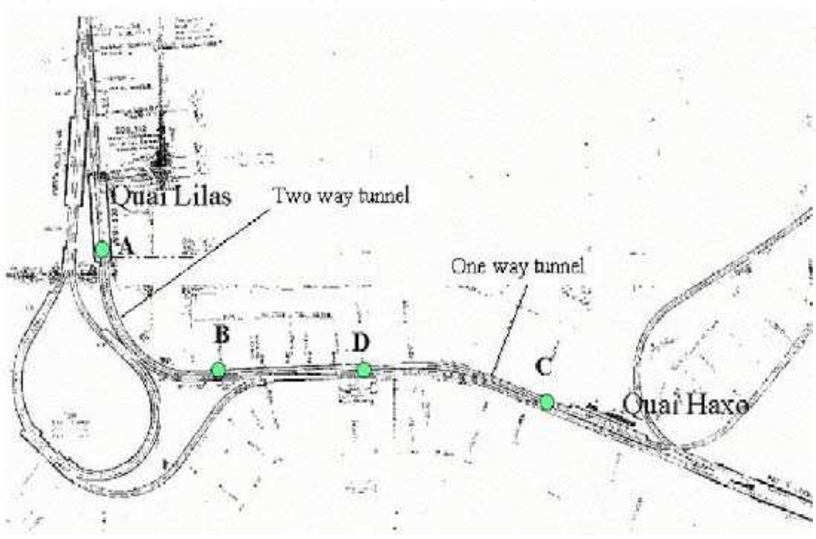

Fig. 14. Plan view of the tunnel. The distance between Quai Lilas and Quai Haxo is 600 m.

For studying a 4x4 MIMO system, 4 horn antennas were located on the platform. On the train, due to operational constraints, the patch antennas had to be placed behind the windscreen. In order to minimize the correlation, these antennas were placed at each corner of the windscreen. The channel sounder was based on a correlation technique and at a center frequency of 900 MHz and a bandwidth of 35 MHz. Both theoretical and experimental approaches have shown that, within this bandwidth, the channel is flat. The complex channel impulse response can thus only be characterized by its complex peak value and the MIMO channel is described in terms of $\boldsymbol{H}$ complex transfer matrices. All details on these measurements can be found in (Lienard et al., 2003).

The orientation of the fixed linear array inside a tunnel is quite critical. Indeed, the correlation distance between array elements is minimized when the alignment of the array elements is perpendicular to the tunnel axis. This result can be easily explained from the interference between active modes giving a signal which fluctuates much more rapidly in the transverse plane than along the tunnel axis. From the measurement of the $\boldsymbol{H}$ matrices, the expected capacity C was calculated for any position of the train moving along the tunnel. If we consider the first 300 m, the fixed array being placed at Quai Lilas, the propagation occurs in the two-track tunnel. Curves in Fig. 15 represent the variation in the cumulative distribution function of C using either a single antenna in transmission and in reception (SISO) or a simple diversity in reception (Single Input Multiple Output – SIMO) based on the maximum ratio combining technique or a 4x4 MIMO technique. These capacities can also be compared to those which would be obtained in a pure Rayleigh channel. In all cases, the signal to noise ratio (SNR) is constant, equal to 10 dB. An increase in capacity when using MIMO is clearly shown in Fig. 15.

Indeed, for a probability of 0.5, *C* is equal to 2, 5 and 9 bit/s/Hz, for SISO, SIMO and MIMO, respectively. In a Rayleigh environment, *C* would be equal to 11 bit/s/Hz.

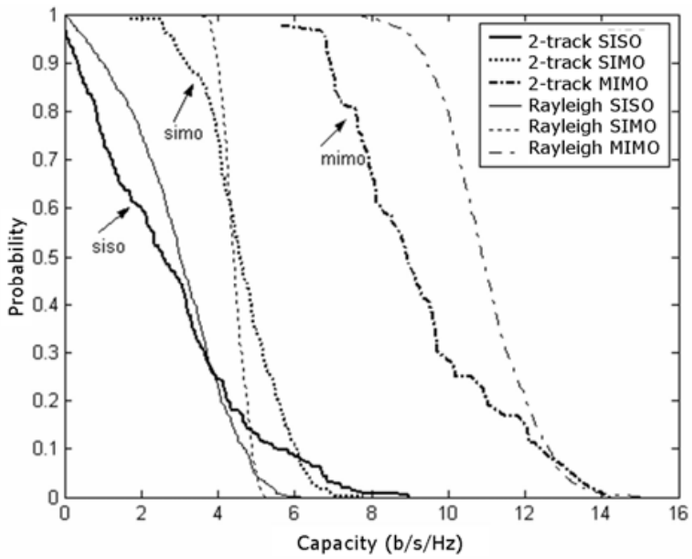

Fig. 15. Cumulative distribution of the capacity in a two-way tunnel for different diversity schemes, for an *SNR* of 10 dB (Lienard et al., 2003).

When the mobile enters the one-track tunnel at point D, one can expect an important decrease in the capacity, even by keeping the same *SNR*. Indeed, as we have seen in 2.1, the high order modes will be strongly attenuated if the tunnel narrows, leading to a decrease in the number of active modes and thus to an increase in the correlation between elements of the mobile array. In Fig. 16, we see that the capacity, in the order of 9 bit/s/Hz in the two-

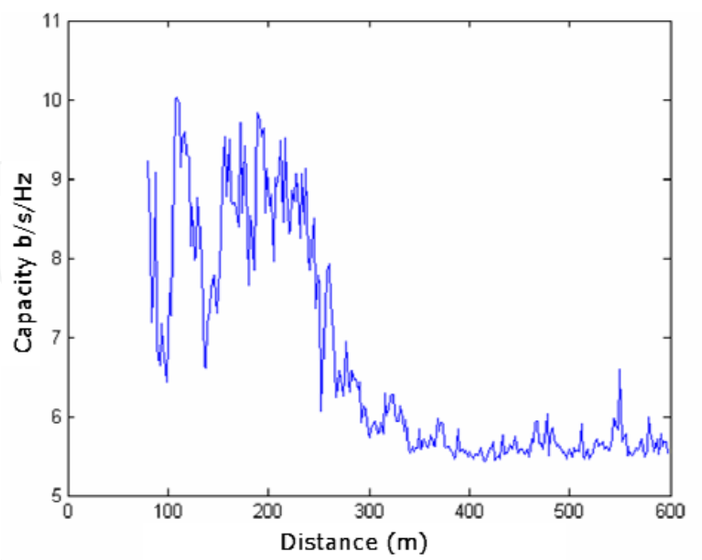

Fig. 16. Capacity for a constant SNR of 10 dB. Transmission from the 2-track tunnel, reception first in the 2-track tunnel (0 - 300 m), and then in the 1-track tunnel (300m – 600m). (Lienard et al., 2006).

track tunnel, decreases to 5.5 bit/s/Hz after the narrowing and thus reaches the capacity of a SIMO configuration. A more detailed explanation based on the correlation coefficients is given in (Lienard et al., 2006).

4.2.2 MIMO capacity in a straight road tunnel and influence of polarization diversity

Let us now consider the straight arched tunnel presented in 3.1.2 and a 4x4 MIMO configuration. In the experiments briefly described in this section, but detailed in (Molina-Garcia-Pardo et al., 2009c), the total length of each array is 18 cm. Different orientations of the elements, i.e. different polarizations, were considered:

1. VV: All Tx and Rx elements are vertically polarized.
2. HH: All Tx and Rx elements are horizontally polarized.
3. VHVH: Both the first and the third elements of each array are vertically polarized, while the second and the fourth elements are horizontally polarized.

In these 3 cases the inter-element spacing is thus equal to 6 cm. Another configuration, called "Dual", because Tx and Rx elements are dual-polarized, was also studied. In this case, the length of the array can be reduced from 18 cm to 6 cm. Channel matrix measurements were made in a frequency band extending from 2.8 to 5 GHz. Since the propagation characteristics do not vary appreciably in this band, average values of the capacity were determined from the experimental data, always assuming a narrow band transmission, i.e. a flat channel. The mean capacity *C* is plotted in Fig. 17 assuming a constant *SNR* of 15 dB, whatever the location of the mobile array. The worst configuration is VV or HH, and is due to the decrease in the number of active modes at large distances, leading to an increase in the correlation between array elements, as previously explained. For VHVH, *C* does not appreciably vary with distance and remains in the order of 16 bit/s/Hz. This better result comes from the low correlation between cross-polarized field components, the distance

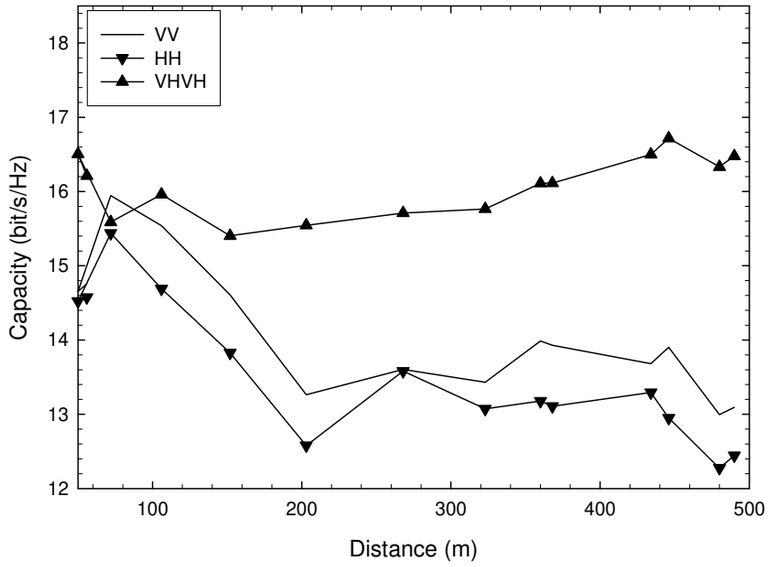

Fig. 17. Mean MIMO capacity assuming a fixed *SNR* at the receiver of 15 dB (Molina-Garcia-Pardo et al., 2009c).

between co-polarized array elements also increasing from 6 cm to 12 cm. A similar result was obtained with the Dual configuration. As a comparison, the theoretical capacity of a 4x4 MIMO in a i.i.d. Rayleigh channel would be around 20 bit/s/Hz, while for a SISO link *C* would be 5 bit/s/Hz, thus much smaller than for MIMO.

These results give some insight into the influence of the number of active modes and of the correlation between array elements on the capacity inside a tunnel. However, in practice, the Tx power is constant and not the *SNR*. Let us thus assume in a next step a fixed Tx power, its value being chosen such that at 500 m and for the VV configuration, an *SNR* of 15 dB is obtained. The capacities for the different array configurations and given in Fig. 18 do not differ very much from one another. This result can be explained by taking both the X-polar discrimination factor and attenuation of the modes into account. First we observe that VV gives slightly better results than HH, the attenuation of the modes corresponding to the vertical polarization being less significant. If we now compare HH and VHVH, we find that the two curves are superimposed. Indeed, we are faced with two phenomena. When using VHVH the spacing between co-polarized array elements is larger than for HH (or VV) and, consequently, the correlation between array elements is smaller. Unfortunately, the waves remain polarized even at large distances, as outlined in Table 3 of 3.1.2. This means that the signal received on a vertical Rx element comes only from the two vertical Tx elements and not from the horizontal Tx elements.

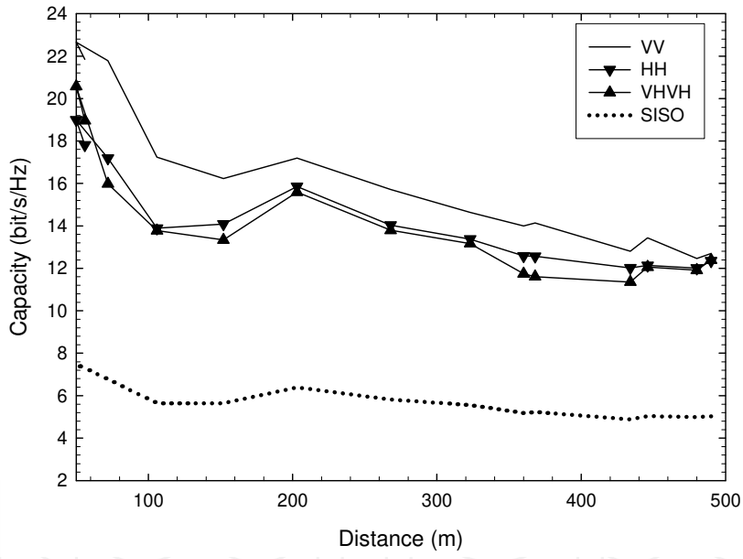

Fig. 18. Mean MIMO capacity assuming a fixed Tx Power (Molina-Garcia-Pardo et al., 2009c).

The total received power in the VHVH configuration is thus nearly half the total power in the HH (or VV) case. It seems that, comparing VHVH and HH, the decrease in power is compensated for by the decrease in correlation, leading to the same capacity. A similar result has been obtained when calculating the capacity of the Dual array. In all cases, the capacity obtained with such MIMO configurations is much larger that the SISO capacity for vertical polarization, as also shown in this figure. In conclusion, changing the polarization of the successive elements of the antenna arrays, as for VHVH, does not result in an improvement in MIMO performance in an arched tunnel. The advantage of the Dual configuration is that it decreases the length of the array while keeping the same channel capacity.

4.3 Performances of MIMO communications schemes

In previous sections, propagation aspects and capacity have been studied, but the bit error rate (BER) is one of the most important system design criterion. The robustness of MIMO to cope with the high correlation between array elements strongly depends on the MIMO architecture. MIMO can be used in three ways: beamforming, spatial multiplexing and space-time coding. Beamforming is useful for increasing the *SNR* and reducing the interference, spatial multiplexing increases the throughput by transmitting the independent flow of data on each antenna, while space time codes decrease the BER. In the following, we will consider space time coding and spatial multiplexing and we will compare the robustness of two well-known architectures, namely Vertical Bell Laboratories Layered Space-Time – VBLAST - (Wolniansky et al., 1998) and Quasi-Orthogonal Space-Time Block Codes – QSTBC - (Tirkkonen et al., 2000; Mecklenbrauker et al., 2004; Tarokh, 1999), assuming a narrow band transmission, i.e. a flat channel. The symbol detection method is based on the Minimum Mean Squared Error (MMSE) algorithm.

The BER was determined from the measurement of the $\boldsymbol{H}$ matrices in the arched tunnel presented in 3.1.2. To be able to carry out a statistical approach, the BER was calculated for numerous Rx locations in the tunnel and for 51 frequencies equally spaced in a 70 MHz band around 3 GHz. In (Sanchis-Borras et al., 2010), two transmission zones were considered: One near Tx, between 50 m and 150 m, and one far from Tx, between 400 and 500 m. In the following, only the results far from Tx are presented. The statistics on the BER were calculated owing to a simulation tool of the MIMO link and by considering 100 000 transmitted symbols, leading to a minimum detectable BER of 10^{-5}. The Tx power is assumed to be constant and was chosen such that a SNR of 10 dB is obtained at 500 m for the VV configuration. To make a fair comparison between MIMO and SISO, chosen as a reference scenario, the throughput and the transmitting power are kept constant in all cases. This means that the modulation schemes are chosen in such a way that the bit rate is the same for SISO and MIMO. In our examples, we have thus chosen a 16QAM scheme for SISO and QSTBC, and a BPSK for 4x4 VBLAST. The complementary cumulative distribution functions (ccdf) of the BER were calculated for the various transmission schemes, MIMO-VBLAST, MIMO-QSTBC and SISO, for two array configurations, VV and Dual. We have chosen these two kinds of array since, as shown in 4.2.2, they present the best performances of capacity under the assumption of constant transmitted power.

The results, presented in Fig. 19, show that there is no benefits from using VBLAST for the VV antenna configuration since the BER (curve 1) does not differ from the BER of a SISO link (curve 5). Despite the fact that the received power with co-polarized Tx and Rx arrays is maximized, the important correlation between the nearest antennas of the Tx/Rx arrays gives rise to a strong increase in the BER. Such a sensitivity of VBLAST to the correlation between antennas was already outlined in (Xin & Zaiping, 2004).

If VBLAST is used, but with dual-polarized antennas (Fig. 19, curve 2), the decrease in correlation allows for a better performance despite the fact that the average received power is smaller. We also note that QSTBC always gives better results than VBLAST. For this QSTBC scheme, contrary to what occurs for VBLAST, the BER is slightly better for VV polarization, i.e. for a higher received power, with QSTBC being much less sensitive to the correlation between antennas than VBLAST.

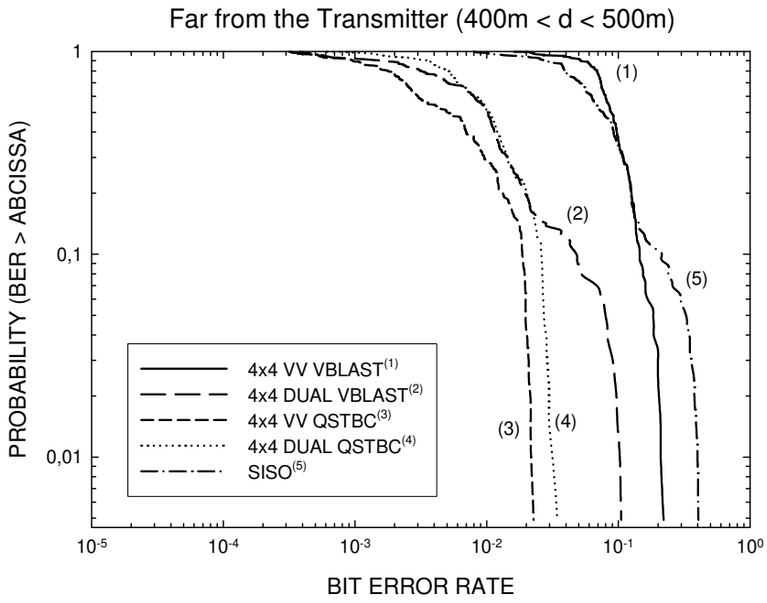

Fig. 19. Complementary cumulative distribution function of the BER far from the transmitter and for a fixed transmitting power (Sanchis-Borras et al., 2010).

As a comparison, we have also calculated the BER for a Rayleigh environment, assuming the same average *SNR* as for VV in tunnel. Dual is not compared to Rayleigh because in tunnel the waves are strongly polarized leading to a non-uniform distribution of the $\boldsymbol{H}$ matrix elements, in contrast to the case of a pure Rayleigh distribution. It appears that results obtained with QSTBC in tunnels are close to those which would be obtained in a Rayleigh environment, even at great distances from Tx. In conclusion, for a communication link in tunnels, MIMO outperforms SISO not only in terms of mutual information but also in terms of BER, assuming of course the same transmitting power and the same throughput, and under the condition that the number of active modes in the receiving plane is sufficient. Due to the guided effect of the tunnel and the attenuation of high order propagating modes at a large distance from the transmitter, the correlation between array elements strongly increases with distance and the QSTBC transmission scheme is thus more appropriate.

5. Concluding remarks

From measurements carried out in a straight tunnel of arched cross-section, which is quite a usual shape, we have shown that experimental results can be interpreted by means of an equivalent rectangular tunnel. The relevance of using MIMO techniques in tunnels was then investigated by first studying the correlation between array elements and the properties of the MIMO channel transfer matrix. This has been done by introducing the concept of active modes existing in the receiving plane. Despite the fact that the waves are guided by the tunnel, leading to a small angular spread for the paths relating the transmitter and the receiver, it appears that MIMO improves the channel capacity owing to a so-called modal diversity. Results obtained in more complex environments were also presented, such as in subway tunnels. In terms of bit error rate with space-time coding, a transmission scheme robust against antenna correlation must be chosen.

6. References

Almers, P.; Tufvesson; F., Karlsson, P. & Molisch, A. (2003). The effect of horizontal array orientation on MIMO channel capacity, *Proc. of the IEEE Vehicular Techno. Conf.*, Vol. 1, pp. 34–38, Seoul, Corea, April 22-25

Arshad, K.; Katsriku, F. A. & Lasebae, A. (2008). Modelling obstructions in straight and curved rectangular tunnels by finite element approach, *J. of Electrical Eng.*, Vol. 59, No. 1, pp. 9-13

Boutin, M.; Benzakour, A.; Despins, C. L. & Affes, S. (2008). Radio wave characterization and modeling in underground mine tunnels, *IEEE Trans. on Antennas and Propag.*, Vol. 56, No. 2, pp. 540 – 549

Chen, S. H. & Jeng, S. K. (1996). BR image approach for radio wave propagation in tunnels with and without traffic, *IEEE Trans. on Vehicular Techno.*, Vol. 45, No. 3, pp. 570-578

Chen, C. H.; Chiu, C. C.; Hung, S. C. & Lin, C.H. (2004). BER performance of wireless BPSK communication system in tunnels with and without traffic, *Wireless Personal Commun.*, Vol. 30, No. 1, pp. 1-12

Correia, L. M. (2006). *Mobile broadband multimedia networks*, Elsevier

Didascalou, D.; Maurer, J. & Wiesbeck, W. (2001). Subway tunnel guided electromagnetic wave propagation at mobile communications frequencies, *IEEE Trans. on Antennas and Propag.*, Vol. 49, No. 11, pp. 1590-1596

Dudley, D. G. (1994). *Mathematical Foundations for Electromagnetic Theory*, IEEE Press, New York

Dudley, D. G.; Lienard, M.; Mahmoud, S. F. & Degauque, P. (2007). Wireless propagation in tunnels, *IEEE Antennas and Propag. Mag.,* Vol. 49, No. 2, pp. 11–26

Emslie, A. G.; Lagace, R. L. & Strong, P. F. (1975). Theory of the propagation of UHF radio waves in coal mine tunnels, *IEEE Trans. on Antennas and Propag.,* Vol. 23, No. 2, pp. 192-205

Foschini, G. J. & Gans, M. J. (1998). On limits of wireless communications in a fading environment when using multiple antennas, *Wireless Personal Commun.*, Vol. 6, No. 3, pp. 311–335

Garcia-Pardo, C.; Molina-Garcia-Pardo, J. M.; Lienard, M. & Degauque, P. (2011). Time domain analysis of propagation channels in tunnels, *Proc. of the 7th Advanced Int. Conf. on Commun.*, St. Maarten, The Netherlands Antilles, March 20 – 25

Hrovat, A.; Kandus, G. & Javornik, T. (2010). Four-slope channel model for path loss prediction in tunnels at 400 MHz, *IET Microw. Antennas Propag.*, , Vol. 4, No. 5, pp. 571–582

Kyritsi, P. & Cox, D. (2002). Expression of MlMO capacity in terms of waveguide modes, *Electronic Letters*, Vol. 38, No. 18, pp. 1056-1057

Laakmann, K. D. & Steier, W. H. (1976). Waveguides: characteristic modes of hollow rectangular dielectric waveguides, *Appl. Opt.*, Vol. 15, pp. 1334–1340

Lienard, M.; Lefeuvre, P. & Degauque, P. (1997). Remarks on the computation of the propagation of high frequency waves in a tunnel, *Annals Telecomm.*, Vol. 52, No. 9-10, pp. 529-533

Lienard, M. & Degauque, P. (1998). Propagation in wide tunnels at 2 GHz: A statistical analysis, *IEEE Trans. on Vehicular Techno.* Vol. 47, No. 4, pp. 1322 - 1328

Lienard, M. & Degauque, P. (2000a). Natural wave propagation in mine environments, *IEEE Trans. on Antennas and Propag.,* Vol. 48, No 9, pp 1326 – 1339

Lienard, M. ; Betrencourt, S. & Degauque, P. (2000b). Propagation in road tunnels: a statistical analysis of the field distribution and impact of the traffic, *Annals of Telecom.,* Vol. 55, No. 11-12, pp. 623-631

Lienard, M.; Degauque, P.; Baudet, J. & Degardin, D. (2003). Investigation on MIMO channels in subway tunnels, *IEEE J. on Selected Areas in Commun*., Vol. 21, No. 3, pp. 332–339

Lienard, M.; Degauque, P. & Laly, P. (2004). A novel communication and radar system for underground railway applications, *European J. of Transport and Infrastructure Research*, Vol. 4, No. 4, pp. 405-415

Lienard, M.; Degauque, P. & Molina-Garcia-Pardo, J. M. (2006). Wave propagation in tunnels in a MIMO context - A theoretical and experimental study, *Comptes Rendus. Phys.,* Vol. 7, pp. 726-734

Loyka, S. (2005). Multiantenna capacities of waveguide and cavity channels, *IEEE Trans. on Vehicular. Techno.,* Vol. 54, pp. 863–872

Mahmoud, S. F. & Wait, J. R. (1974). Geometrical optical approach for electromagnetic wave propagation in rectangular mine tunnels, *Radio Science*, Vol. 9, pp. 1147–1158

Mahmoud, S. F. (1988). *Electromagnetic waveguides theory and applications*, Peter Pergrenus Ed.

Mahmoud, S. F. (2008). Guided mode propagation in tunnels with non-circular cross section, *Proc. of the IEEE Int. Symp. on Antennas and Propag.,* San Diego, USA, July 5-11

Mahmoud, S. F. (2010). *Wireless transmission in tunnels,* Chapter 1 in the book *Mobile and Wireless Communications*, InTech, ISBN 978-953-307-043-8

Mariage, P.; Lienard, M. & Degauque, P. (1994). Theoretical and experimental approach of the propagation of high frequency waves in road tunnels, *IEEE Trans. on Antennas and Propag.,* Vol. 42, No. 1, pp. 75-81

Marti Pallares, F.; Ponce Juan, F. J. & Juan-Llacer, L. (2001). Analysis of path loss and delay spread at 900 MHz and 2.1 GHz while entering tunnels, *IEEE Trans. on Vehicular Techno.,* Vol. 50, No.3, pp. 767-776

Mecklenbrauker, C. F. & Rupp, M. (2004). Generalized Alamouti codes for trading quality of service against data rate in MIMO UMTS, *EURASIP J. on Applied Signal Processing*, No. 5, pp. 662–675

Molina-Garcia-Pardo, J. M.; Rodríguez, J. V. & Juan-Llácer, L. (2003). Angular Spread at 2.1 GHz while entering tunnels, *Microwave and Optical Technology Letters*, Vol. 37, No. 3, pp. 196-198

Molina-García-Pardo, J. M.; Rodríguez, J. V. & Juan-Llacer, L. (2004). Wide-band measurements and characterization at 2.1 GHz while entering in a small tunnel, *IEEE Trans. on Vehicular Techno.,* Vol. 53, No. 6, pp. 1794-1799

Molina-Garcia-Pardo, J. M.; Lienard, M.; Degauque, P.; Dudley, D. G. & Juan Llacer, L. (2008a). Interpretation of MIMO channel characteristics in rectangular tunnels from modal theory, *IEEE Trans. on Vehicular Techno*., Vol. 57, No. 3, pp. 1974-1979

Molina-Garcia-Pardo, J. M.; Nasr, A.; Liénard, L.; Degauque, P. & Juan-Llácer, L. (2008b). Modelling and understanding MIMO propagation in tunnels, *Proc. of 2nd International Conf. on Wireless Communications in Underground and Confined Areas* Val-d'Or, Québec, Canada, August 25-27

Molina-Garcia-Pardo, J. M.; Lienard, M.; Nasr, A. & Degauque, P. (2008c). On the possibility of interpreting field variations and polarization in arched tunnels using a model for propagation in rectangular or circular tunnels, *IEEE Trans. on Antennas and Propag*., Vol. 56, No. 4, pp. 1206–1211

Molina-Garcia-Pardo, J. M.; Lienard, M.; Stefanut, P. & Degauque, P. (2009a). Modelling and understanding MIMO propagation in tunnels, *J. of Communications*, Vol. 4, No. 4, pp. 241-247

Molina-Garcia-Pardo, J. M.; Lienard, M.; Degauque, P.; Simon, E. & Juan Llacer, L. (2009b) On MIMO channel capacity in tunnels, *IEEE Trans. on Antennas and Propag.*, Vol. 57, No. 11, pp. 3697-3701

Molina-Garcia-Pardo, J. M.; Lienard, M.; Degauque, P.; García-Pardo, C. & Juan-Llacer, L. (2009c). MIMO channel capacity with polarization diversity in arched tunnels, *IEEE Antennas and Wireless Propagation Letters*, Vol. 8, pp. 1186-1189

Molina-Garcia-Pardo, J. M.; Lienard, M. & Degauque, P. (2009d). Propagation in tunnels: experimental investigations and channel modeling in a wide frequency band for MIMO applications, *EURASIP J. on Wireless Commun. and Networking*, Article ID 560571, 9 pages, doi:10.1155/2009/560571

Molisch, A. F. (2005), *Wireless communications*, IEEE Press

Popov, A. V. & Zhu, N. Y. (2000). Modeling radio wave propagation in tunnels with a vectorial parabolic equation, *IEEE Trans on Antennas and Propag.*, Vol. 48, No. 9, pp. 1316 - 1325

Rappaport, T. S. (1996). *Wireless communications: Principles and practice*, Prentice Hall Ed.

Sanchis-Borras, C.; Molina-Garcia-Pardo, J. M.; Lienard, M.; Degauque, P. & Juan LLacer, L. (2010). Performance of QSTBC and VBLAST algorithms for MIMO channels in tunnels, *IEEE Antennas and Wireless Propag. Letters*, Vol. 9, pp. 906-909

Siy Ching, G.; Ghoraishi, M.; Landmann, M.; Lertsirisopon, N.; Takada, J.; Imai, T.; Sameda, L. & Sakamoto, H. (2009). Wideband polarimetric directional propagation channel analysis inside an arched tunnel, *IEEE Trans. on Antennas and Propag.*, Vol. 57, No. 3, pp. 760 – 767

Tarokh, V.; Jafarkhani, H. & Calderbank, A. R. (1999). Space-Time block codes from orthogonal designs, *IEEE Trans. on Information Theory*, Vol. 45, pp. 1456-1467

Telatar, I. E. (1995). Capacity of multi-antenna gaussian channel, *European Trans. on Telecom.*, Vol. 10, pp. 585–595

Therrien, C. W. (1992). *Discrete Random Signals and Statistical Signal Processing*, Prentice Hall, Englewood Cliffs, New Jersey

Tirkkonen, O.; Boariu, O. & Hottinen, A. (2000). Minimal nonorthogonality rate one space time block codes for 3+ Tx antennas, *Proc. of the IEEE 6th Int. Symp. on Spread-Spectrum Tech. & Appli.*, pp. 429 – 432, New Jersey, USA, Sept. 6-8

Valdesuerio, A.; Izquierdo, B. & Romeu, J. (2010). On 2x2 MIMO observable capacity in subway tunnels at X-Band: an experimental approach, *IEEE Antennas and Wireless Propag. Letters,* Vol. 9, pp. 1099-1102

Wait, J. R. (1962). *Electromagnetic waves in stratified media*, Pergamon Press

Wang, T. S. & Yang, C. F. (2006). Simulations and measurements of wave propagation in curved road tunnels for signals from GSM base stations, *IEEE Trans. on Antennas and Propag.*, Vol. 54, No. 9, pp. 2577-2584

Wolniansky, P. W.; Foschini, G. J.; Golden, G. D. & Valenzuela, R. A. (1998). V-BLAST: An architecture for realizing very high data rates over the rich-scattering wireless channel, *Proc. of the URSI Symposium on Signals Systems and Electronics*, pp. 295-300

Xin, L. & Zaiping N. (2004). Performance losses in V-BLAST due to correlation. *IEEE Antennas and Wireless Propagation Letters*, Vol. 3, pp. 291-294

Yamaguchi, Y.; Abe, T. & Sekiguchi, T. (1989). Radio wave propagation loss in the VHF to microwave region due to vehicles in tunnels, *IEEE Trans. on Electromagn. Compat.*, Vol. 31, No. 1, pp. 87-91

Zhang, Y. P.; Zheng, G. X. & Sheng, J. H. (2001). Radio propagation at 900 MHz in underground coal mines, *IEEE Trans. on Antennas and Propag.*, Vol. 49, No. 5, pp. 757–762

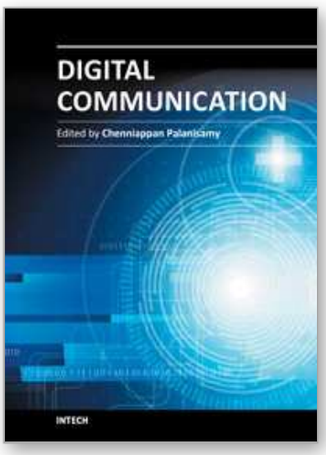

Digital Communication

Edited by Prof. C Palanisamy

ISBN 978-953-51-0215-1
Hard cover, 208 pages
Publisher InTech
Published online 07, March, 2012
Published in print edition March, 2012

All marketing is digital and everyone should have a digital strategy. Everything is going mobile. "The world has never been more social" is the recent talk in the community. Digital Communication is the key enabler of that. Digital information tends to be far more resistant to transmit and interpret errors than information symbolized in an analog medium. This accounts for the clarity of digitally-encoded telephone connections, compact audio disks, and much of the enthusiasm in the engineering community for digital communications technology. A contemporary and comprehensive coverage of the field of digital communication, this book explores modern digital communication techniques. The purpose of this book is to extend and update the knowledge of the reader in the dynamically changing field of digital communication.

How to reference

In order to correctly reference this scholarly work, feel free to copy and paste the following:

Jose-Maria Molina-Garcia-Pardo, Martine Lienard and Pierre Degauque (2012). Wireless Communication in Tunnels, Digital Communication, Prof. C Palanisamy (Ed.), ISBN: 978-953-51-0215-1, InTech, Available from: http://www.intechopen.com/books/digital-communication/wireless-communication-in-tunnels

INTECH
open science | open minds

InTech Europe
University Campus STeP Ri
Slavka Krautzeka 83/A
51000 Rijeka, Croatia
Phone: +385 (51) 770 447
Fax: +385 (51) 686 166
www.intechopen.com

InTech China
Unit 405, Office Block, Hotel Equatorial Shanghai
No.65, Yan An Road (West), Shanghai, 200040, China
中国上海市延安西路65号上海国际贵都大饭店办公楼405单元
Phone: +86-21-62489820
Fax: +86-21-62489821

IntechOpen